International Journal of Pharmaceutics 661 (2024) 124380

Contents lists available at ScienceDirect

International Journal of Pharmaceutics

journal homepage: www.elsevier.com/locate/ijpharm

Bioactive pH-sensitive nanoemulsion in melanoma cell lines

Jacopo Forte [a,*], Maria Gioia Fabiano [a], Maria Grazia Ammendolia [b], Rossella Puglisi [c,*], Federica Rinaldi [a,*], Caterina Ricci [d], Elena Del Favero [d], Maria Carafa [a], Gianfranco Mattia [c,1], Carlotta Marianecci [a,1]

[a] Department of Drug Chemistry and Technology, Sapienza University of Rome, Rome 00161, Italy
[b] National Center for Innovative Technologies in Public Health, Istituto Superiore di Sanità, Rome 00161, Italy
[c] Center for Gender-specific Medicine, Istituto Superiore di Sanità, 00161 Rome, Italy
[d] Dipartimento di Biotecnologie Mediche e Medicina Traslazionale, Università di Milano, Milan, Italy

ARTICLE INFO

Keywords:
Drug delivery
Nanoemulsions
pH sensitivity
Curcumin
Melanoma
Metastatization

ABSTRACT

Melanoma is an aggressive form of skin cancer with elevated propensity to metastasize. One of the major critical issues in the treatment of oncological patients is represented by the development of toxicity and resistance to the available therapies. Great progress has been made in the field of nanotechnologies to limit the unwanted effects of anti-cancer treatments. We explored the potential of creating oil-in-water nanoemulsions composed of oleic acid, as a bioactive carrier for lipophilic drug delivery. This bioactive nanoemulsion was loaded with Curcumin, a natural fluorescent lipophilic compound, used as a model drug to evaluate nanoemulsion capability to: i) encapsulate the lipophilic moiety; ii) interact with the specific cells, and iii) improve the efficacy of the loaded model drug compared to the free one. Therefore, we evaluated the physical–chemical features of Curcumin-loaded nanoemulsions, confirming their pH sensibility and their stability over time. Moreover, the nanoemulsions were able to preserve the loaded Curcumin by degradation/destabilization phenomena. Finally, we verified some of the biological functions of Curcumin delivered by nanoemulsions in the B16F10 melanoma cell line. We obtained evidence of the biological action of Curcumin, suggesting oleic-based nanoemulsions as an efficient nanocarrier for lipophilic drug delivery.

1. Introduction

Melanoma is the most severe form of skin cancer. At the advanced stage, beyond the high propensity to metastasize in other organs, including the lung and the brain, this tumor is prevalently unresponsive to conventional chemotherapy and radiotherapy. Furthermore, melanoma develops resistance after biologically targeted therapy (Rambow et al., 2019; Whiteside, 2008). Although the recent advent of immunotherapy has increased the chance of treatment for patients with advanced forms of the disease (stage III and IV), a significant percentage of them are forced to interrupt therapies either for severe secondary effects or drug resistance (Jessurun et al., 2017).

The continuous progress in the field of nanomedicine and nanotechnology and understanding of cell and tumor biology have improved the possible strategies for the diagnosis, treatment, and management of cancer. Drug delivery systems could enhance the efficiency of pharmacological therapy reducing drug resistance, systemic toxicity and dosage, enhancing the short half-life or poor bioavailability of the active compound. Moreover, several approaches have been explored to selectively deliver active compounds directly to the tumor site developing a drug delivery system (DDS) able to ameliorate the stability, bioavailability, accumulation, and penetration of the loaded drug into the tumor tissue. Several nanocarriers could be proposed for the administration of drugs or natural compounds as non-conventional therapy, such as liposomes, niosomes, polymeric nanoparticles, or nanoemulsions (Pandey et al., 2021; Song et al., 2021). Oil-in-water (O/A) nanoemulsions are a promising option for drug delivery systems due to their ability to solubilize lipophilic active compounds and their significant stability over

* Corresponding authors.
E-mail addresses: jacopo.forte@uniroma.it (J. Forte), mariagioia.fabiano@uniroma1.it (M. Gioia Fabiano), maria.ammendolia@iss.it (M. Grazia Ammendolia), rossella.puglisi@iss.it (R. Puglisi), federica.rinaldi@uniroma1.it (F. Rinaldi), caterina.ricci@unimi.it (C. Ricci), elena.delfavero@unimi.it (E. Del Favero), maria.carafa@uniroma1.it (M. Carafa), gianfranco.mattia@iss.it (G. Mattia), carlotta.marianecci@uniroma1.it (C. Marianecci).
[1] **These authors shared seniorship.**

https://doi.org/10.1016/j.ijpharm.2024.124380
Received 11 April 2024; Received in revised form 21 June 2024; Accepted 22 June 2024
Available online 29 June 2024

time. Additionally, the properties of the oil in the nanoemulsion (NEs) can enhance the activity of the overall structure and improve the effectiveness of the entrapped drug. A crucial step is the choice of the NEs components to design and obtain nanocarriers with specific physical–chemical features able to produce the desired effect. Moreover, the components and the preparation method are generally simple and with low costs, fundamental characteristics for a possible scale-up of pharmaceutical production (Rosner et al., 2006). Encapsulation of active compounds in NEs could represent a promising approach to tackling the advanced stages of melanoma (Qiu et al., 2014). Unfortunately, the absence of tumor-specific antigens on melanoma cells makes it difficult to achieve a selective cell targeting of the drug-loaded nanocarriers. To bypass this problem one promising approach is the development of nanocarriers that can be triggered to release the anticancer active compound in response to specific chemical stimuli such as the low pH present in the tumor microenvironment (TME). The hypoxic conditions of the tumor cells produce an excess of lactate that is released in the TME along with other acidic materials, establishing an acidic environment (Warburg effect). Thus, the pH of tumors can decrease to 5.7 compared to the pH of 7.4 of the healthy tissues (Stubbs et al., 2000). In this context, our previous studies demonstrated that the improved cellular concentration of Oleic Acid (OA), obtained overexpressing the desaturase enzyme SCD5 (Stearoyl CoA desaturase 5) in melanoma cells, reduced the malignant features either of melanoma cells or of the tumor microenvironment (Bellenghi et al., 2015 Jul; Puglisi et al., 2018). These results suggest the potential use of OA as a new strategy against melanoma. To overcome the high viscosity of OA which hampers its administration *in vivo*, we recently developed OA based NEs (NEsO) (Rinaldi et al., 2022a). In addition to its antimetastatic role, OA is characterized by high pH-sensitiveness, thus conferring to NEsO the ability to release the drug content in the acidic tumor microenvironment. The NEsO formulation, thanks to their versatility and physicalchemical features, could be employed for topical application (after inclusion of the NEsO suspension semi-solid dosage forms), parenteral or nasal administration. Considering the melanoma propensity to metastasize mainly to the lungs, the chance of drug aerosolization represents an appealing therapeutic strategy for safer lung metastasis management.

Curcumin, a natural polyphenol extracted from the rhizomes of the plant *Curcuma longa* (turmeric), is characterized by several pharmacological properties including anti-oxidant, anti-inflammatory, anti-diabetic, and anti-atherosclerotic. Furthermore, some anti-cancer activities, such as the inhibition of the growth, invasion, migration ability and induction of apoptosis have been described (Liu et al., 2009; Lu et al., 2014; Mirzaei et al., 2016; Wang et al., 2015; Xue et al., 2014). Both, Curcumin loading and appropriate experimental design, could represent an efficient strategy to predict the *in vivo* nanocarrier efficacy. The Curcumin, used as model drug and at the same time as fluorescent probe, can give information about the nanocarrier *in vitro* capability to interact with the selected cells, and it is also useful to assess the improved efficacy of the loaded model drug respect to the free one (Parchekani et al., 2022).

Therefore, we prepared and characterized Curcumin loaded NEsO (NEsOCur) and we deeply studied the morphological and structural features of the NEsOCur (hydrodynamic diameter, ζ-potential, polydispersion index (PDI), stability, morphology, microviscosity, polarity, and pH-sensitivity). In addition, release studies in Hepes buffer and different media were also carried out. The fluorescent nature of Curcumin allowed us to evaluate NEsOCur interaction with the cells. Thus, the cellular uptake of the Curcumin contained in the NEsO and its long-lasting maintenance were analyzed by flow cytometric analysis, whereas the intracellular distribution of internalized Curcumin was evaluated by confocal microscopy analysis. Finally, the *in vitro* effect of Curcumin loaded NEsO on mouse B16F10 melanoma cells was verified by evaluating cell proliferation and apoptosis. Overall, in this work we demonstrated that NEsO can entrap Curcumin without modifying their chemical and physical characteristics and the Cur entrapment increases its *in vitro* cell bioavailability. These results indicate that NEsO are good candidate for *in vivo* studies. In particular, future perspectives will be to develop NEsO loaded with anticancer lipophilic drugs/active compounds to test *in vivo* study in a model of melanoma constituted by B16F10 cells in syngeneic C57Bl/6 mice.

2. Materials and methods

2.1. Materials

Polysorbate 80 (Tween-80), Oleic Acid, Curcumin, Hepes salt {N-(2-hydroxyethyl), piperazine-N-(2-ethane sulphonic acid)}, diphenylhexatriene (DPH), Pyrene, Sodium Acetate, Acetic Acid Glacial were Sigma-Aldrich products (Sigma-Aldrich, Milan, Italy). Ethanol and all other products and reagents were of analytical grade. Dulbecco's modified Eagle's medium (DMEM, 61965–026), fetal bovine serum (FBS, 10270–106) and Dulbecco's Phosphate Buffered Saline (DPBS1X) were GIBCO (Thermo Fisher Scientific Inc., USA), Cell proliferation kit II (XTT, Roche, 33324 Mannheim, Germany). TO-PRO-3 Iodide (T3605, Thermo Fisher Scientific Inc., USA) Paraformaldehyde solution 4 % in PBS (PFA 4 %, Chem Cruz, Santa Cruz Biotechnology, Inc.), ProLong (P36930, Invitrogen, UK), Hoechst 33,342 (H3570, Invitrogen, UK). NuPAGE Bis-Tris protein gels (NP0301BOX, Invitrogen, UK) Antibody: p21 (Santa Cruz Biotechnology, INC sc-817), PCNA (clone 2G7, TA800875 Origene), Caspase-3 (Cell Signaling, #9665) and β-actin (Clone AC-15 #A5441).

2.2. Preparation of nanoemulsions

According to Rinaldi et al. 2022 (Rinaldi et al., 2022a), to allow NEs formation, the selected compounds (Table 1) were vortexed vigorously for 1 min to ensure mixing, analyzed by visual inspection and then sonicated for 10 min at 25° C, using a tapered microtip, operating at 20 kHz at an amplitude of 20 % (Vibracell-VCX 400, Sonics, Taunton, MA, USA) to obtain the desired Oil-in-Water NEs. Finally, filtration was performed (MF-Millipore®, Ireland, E.U. 0.22 μm) to retain impurities and to sterilize the sample as established by Ph. Eur.

2.3. Dynamic light scattering and ζ-potential measurements

Hydrodynamic diameter, ζ-potential and polydispersity index (PDI) of empty and loaded NEs were evaluated using Malvern Nano ZS90 apparatus (Malvern Instruments, Worcestershire, UK), equipped with a 5 mW HeNe laser, $\lambda = 632.8$ nm. The scattering angle was 90° and the analysis of the intensity autocorrelation function was carried out using Contin algorithm. The calculated mean hydrodynamic radius corresponds to the intensity weighted average (Kunwar et al., 2008). Electrophoretic mobility of the vesicles was measured by laser Doppler anemometry using the Malvern Zetasizer Nano ZS90 apparatus (Malvern Instruments, Worcestershire, UK). The ζ-potential was obtained by converting the mobility (u) using the Smoluchowski relation $\zeta = u\eta/\delta$, where η is the viscosity and the permittivity of the solvent phase (Sennato et al., 2005).

2.4. Transmission electron microscopy (TEM)

The morphology of NEsOCur, at two different pH values (pH 7.4 and pH 5.5), was characterized by TEM. Samples were diluted ten times in the respective buffers and dripped onto a formwar/carbon-coated copper grid. After dying with 2 wt% phosphotungstic acid (PTA) solution

Table 1
Qualitative and quantitative (mg/ml) composition of NEsOCur.

Sample	Tween 80 (mg/ml)	Oleic Acid (mg/ml)	Curcumin (mg/ml)
NEsOCur	19.6	19.6	1.0

(pH 7.2), they were dried in the air. Droplets were then observed by a FEI 280S transmission electron microscopy (FEI Company, Hillsboro, OR, USA), at an accelerating voltage of 100 kV. Photographs were taken by the Mega-view II SIS camera (Olympus, Hamburg, Germany) and the Adobe Photoshop software (Adobe, San Jose, CA, USA) was used to optimize image editing.

2.5. pH-sensitivity evaluation

pH sensitivity experiments were carried out using different fluorescent probes, such as DPH and Pyrene. By fluorescence spectroscopy, using spectrofluorometer LS5013, PerkinElmer, MA, USA, the characteristics of NEs at different pH values were investigated. The behavior of probe loaded nanosystems is strongly influenced by the inner structure of the nanodroplet, therefore, the structure destabilization at different pH will determine a modification of the emission signals of the probes (Rinaldi et al., 2022a).

DPH provides information on the fluidity variation of the oil nanodroplets following the pH variation of the external environment (Manosroi et al., 2003). Fluorescence measurements were performed with excitation λex = 350 nm and detecting the fluorescence intensity at λem = 428 nm, using a luminescence spectrometer (LS5013, PerkinElmer, Waltham, MA, USA) (Sciolla et al., 2021).

The fluorescence anisotropy (A) was determined using the equation (1):

$$Fluorescenceanisotropy(A) = \frac{(I_{vv} - I_{vh})xG}{(I_{vv} + 2I_{vh})xG} \quad (1)$$

where I_{VV}, I_{VH}, I_{HV} and I_{HH} are the intensities of the fluorescence measured by a LS5013 PerkinElmer spectrophotometer (Forte et al., 2023), with V (vertical) and H (horizontal) orientation of the polarized light.

$G = I_{HV}/I_{HH}$ factor is the ratio of sensitivity of the detection system. Results are shown as the average of three different preparations ± standard deviation. The anisotropy value is correlated to the microviscosity of the system near the probe and is inversely proportional to the fluidity of the nanosystem (Lentz, 1989).

On the other hand, Pyrene was added inside nanocarrier together with lipophilic compounds maintaining the same preparation method previously described in section 2.2; this fluorescent probe is distinguished by a spectrum characterized by five emission bands (I_1-I_5) as monomer and one as excimer (I_E). Intensities of these peaks depend on the mobility and lateral distribution of the probe within the oily phase (Le Guyader et al., 2007). The signals emitted by the sample were recorded with an emission spectrum with λ = 350–550 nm and λex = 330 nm. Relationship between the different intensities provides indications regarding the microviscosity and the polarity. In particular, the I_1/I_3 ratio, corresponding to the first and third vibration bands of the Pyrene spectrum, is linked to the polarity of the probe environment. While the I_E/I_3 ratio characterizes the microviscosity of the nanosystem; in fact, depending on the viscosity, the pyrene can organize itself and form the intramolecular excimer (Zachariasse, 1978).

2.6. Small angle X-ray scattering

SAXS measurements were performed at the European Synchrotron Radiation Facility at the BM26 beamline Grenoble, France. A Pilatus 1 M detector (Dectris, Baden, Switzerland) with a pixel size of 172 μm × 172 μm is placed at a distance of 1.4 m to acquire 2D SAXS images. The beamline is operated at a photon energy of 12 keV, corresponding to an X-ray wavelength of λ = 1.033 Å and calibrated using and silver behenate. The measurements were acquired for 10 s. The SAXS q range ($q = (4\pi/\lambda)\sin(\theta/2)$), went from 0.1 to 6. The 2D SAXS images were integrated in the pyFAI program and 1D profiles were obtained in the q = $(4\pi/\lambda)\sin(\theta/2)$ range 0.1–6 nm^{-1}, where θ is the scattering angle. The raw data were normalized for the intensity of the X-ray beam and corrected for detector sensitivity prior to background correction. After background subtraction, SAXS intensity profiles provide information on the shape and internal arrangement of nano-structures and on structural changes upon pH variation, if any (Barattin et al., 2018).

2.7. Drugs entrapment efficiency (EE%)

UV–Vis spectrometer (Lambda 25, PerkinElmer, Waltham, MA, USA) was employed to evaluate the amount of Curcumin actually entrapped in NEs (Entrapment Efficiency, E.E.). The absorbance of Curcumin at λ = 430 nm was measured by diluting NEs in Ethanol:Hepes 1:1 (vol:vol) and E.E. % is obtained using the Curcumin calibration curve and the following equation (2):

$$E.E.(\%) = \frac{Entrappeddrug(mg)}{Totaldrugused(mg)} \times 100 \quad (2)$$

2.8. Physicochemical stability

Stability studies were carried out over time on NEsOCur, stored at room temperature (25 °C) and 4 °C for 90 days. Measurements were made at definite time intervals (1, 30, 60, and 90 days) by DLS (Malvern Instruments, Worcestershire, UK) to assess the possible variations of the size and the ζ-potential during the considered time interval (Rinaldi et al., 2022b). Moreover, the Curcumin stability as free Curcumin in solution (free Curcumin solubilized in a mixture of Etanol:Hepes 50:50 (vol:vol)) and as Curcumin-loaded NEsO was evaluated over time. This experiment consists in observing over time the possible intensity and shape variations of the Curcumin peak by a UV–vis spectrometer (Lambda 25, PerkinElmer, Waltham, MA, USA), at λ = 430 (Ke et al., 2011).

As preliminary biological evaluation, the *in vitro* stability of NEsO and NEsOCur in the presence of DMEM-FBS culture medium has been carried out. 1 mL of NEsO or NEsOCur was added to 1 mL of DMEM-FBS culture medium and put into a test tube, subject to a magnetic stirrer at 37 °C. The average size was evaluated by means of DLS maintaining samples at 37 °C and performing measurements at different time points (every hour for 8 h and then after 12, 24, 48 and 72 h).

2.9. In vitro release studies

In vitro Curcumin release from NEsOCur was carried out using a dialysis membrane (molecular weight cut-off: 8000 MW by Spectra/Por®) at 37 °C until up to 72 h in Hepes buffer (pH 7.4, 0.02 M) and Acetate buffer (pH 5.5, 0.2 M).

At predetermined time intervals, aliquots of 1 ml of external medium (composed by 50 % etanol and 50 % Hepes buffer) were taken and analyzed, by UV-analysis and then re-inserted back in the external medium. Curcumin release by NEs was analyzed using a UV spectrophotometer (Lambda 25, PerkinElmer, Waltham, MA, USA), using Curcumin absorbance at λ = 430. All release experiments were carried out in triplicate.

2.10. Cell cultures

Mouse melanoma cell line B16F10 was kindly gifted by MP Colombo (Istituto Nazionale Tumori di Milano, Italy). Human melanoma cell line A375M was previously described (Rinaldi et al., 2022a). All cell lines were cultured in DMEM supplemented with 10 % FBS and maintained in a humified incubator (5 % CO2, 37 °C). Melanoma cell lines were periodically tested for mycoplasma contamination with MycoAlert kit (LT07-418, Lonza) before use.

2.11. Flow cytometry

Curcumin cellular uptake was evaluated by flow cytometry (FCM). Briefly, cells seeded on 6-well culture plate in DMEM 10 % FBS v/v, were treated with Curcumin loaded NEsO and free Curcumin solubilized in DMSO (free Cur) at concentration of 13.5 and 6.75 μM respectively. At each time point (5, 24 and 48 h), cells were trypsinized and washed twice in PBS1X. A proper number of cells were stained with TOPRO (λex 642/ λem 661 nm, bound to nucleic acid) to evaluate the uptake in live cells (TOPRO blue negative cells). Cells were analysed for Curcumin emission (λex 425/ λem 530 nm) by CytoFLEX LX Flow Cytometer (UV-Violet-Blue-Yellow Green-Red (U-V-B-Y-R) Series, Beckman Coulter), and data were analysed with Kaluza Analysis Software (Beckman Coulter).

2.12. Confocal microscopy

To visualize nanocarrier cellular internalization, B16F10 cells were seeded in chamber slides and subsequently exposed to NEsOCur (13.5 μM) or to the corresponding dose of free Cur. After 24 h of incubation, cells were fixed in PFA 4 %, washed in DPBS1X, and nuclei stained with Hoechst 33342. Finally, slides were mounted with ProLong Gold Antifade Reagent and analysed by Olympus F1000 laser-scanning confocal microscopy (Olympus, Tokyo, Japan).

2.13. Cell proliferation studies

A proper number of cells was seeded in a 96-well culture plate in DMEM 10 % FBS v/v (day 0) and treated with increased amounts of NEsOCur (3.75, 4.5, 6.75 and 13.5 μM) or free Cur for different time points (day 1, 2 and day 3). At each time point, the cell culture was stopped and the proliferation index was evaluated by using cell proliferation kit II (XTT) according to manufacturing procedures (Rinaldi et al., 2022a). The orange formazan dye formed by metabolic active cells was spectrophotometrically quantified (Victor X3, Wallac-Perkin-Elmer 2030 Software v. 4 00) at 490 nm. The values measured for treated cells were compared to those of untreated controls.

2.14. Western blot analysis

Western blots were performed according to standard procedures. Total proteins were isolated from cell lysates by using NP40 cell lysis buffer and separated by the precast NuPAGE polyacrylamide gel system (Life Technologies Carlsbad, CA, USA). Protein concentration was measured by the Bradford protein assay (Biorad Hercules, CA, USA).

2.15. Statistical analysis

The results are shown as the means of three independent experiments ± standard deviation (S.D.). The data were evaluated for statistical significance using the Student's *t*-test of Excel (Microsoft Office Professional Plus 2019) and one-way analysis of variance (ANOVA). Any p value < 0.05 was considered statistically significant.

3. Results and discussion

In the last decade, several delivery systems such as nanoparticles have been developed to greatly increase the bioavailability of Curcumin thereby potentiating its biological effects (Tomeh et al., 2019).

Recently, we have prepared and characterized pH-sensitive OA-based nanoemulsions, potentially able to target the drugs to tumoral acidic microenvironment. This work aimed to demonstrate the capability of OA-nanoemulsions to load a lipophilic drug, such as Curcumin, here employed as a model drug, and to interact with the murine melanoma cells, affecting tumor cell activity *in vitro*.

To study and confirm the pH sensitivity of NEsO prepared with Curcumin, NEsOCur was characterized in terms of mean diameter, polydispersity index (PDI), and ζ-potential, at two different pH: pH 7.4 (Hepes buffer) and pH 5.5 (Acetate buffer). Moreover, the entrapment efficiency of Curcumin was studied. The obtained data reported in Table 2, demonstrate that, as expected, drug loading (E.E.% almost 100 % for both pH condition) causes an increase in droplet particle size concerning the empty ones (from 104 nm to 122 nm) (Rinaldi et al., 2022a), with the same polydispersity (PDI 0.27) and ζ-potential values. At pH 5.5 NEsOCur showed preserved integrity, increased size and PDI, and a decrease of ζ-potential value, as reported in Table 2. The structural rearrangement of NEsOCur, at acidic pH, can be induced by Oleic Acid and Tween 80 pH-sensitive components, as suggested for the NEsO system (Makhathini et al., 2022; (Rinaldi et al., 2022a). The increased size has been observed and justified by multidisciplinary techniques, in fact fluorescence and spectrophotometric measurements (employing different lipophilic fluorescent probes), SAXS and TEM analyses (described and discussed below), suggest structural changes of the NEs (at pH 5,5) probably due to the presence of pH-sensitive molecules (Tween 80 and OA). In particular, the chemical stability of polysorbates due to hydrolysis phenomena, can affect the integrity of nanocarriers. Tween-80 is susceptible to destabilization by environment factors, such as pH, temperature and ionic strength. Partial chemical hydrolysis of Tween 80 can be promoted by acidic condition, with consequent nanoemulsions rearrangement, promotion of water adsorption, perturbation of the oil droplet with size and PDI increase (Dwivedi et al., 2020, Stefanidis and Jencks, 1993, Prajapati et al., 2020). Taking into account at pH 5.5, ζ-potential measurements were influenced by the buffer characteristics (Rinaldi et al., 2022a) ".

Lipophilic features such as fluidity, polarity and microviscosity of the NEsOCur nanodroplets were investigated employing different fluorescent probes (DPH and Pyrene), as described in 2.5 section, and obtained results were reported in Table 3. Anisotropy values of empty and Curcumin loaded NEsO were quite similar (0.14–0.17 respectively) (Rinaldi et al., 2022a), indicating that the presence of Curcumin does not influence the fluidity of NEsO, probably because it is appropriately solubilized in the oil phase. On the contrary, sample polarity and microviscosity change after the Curcumin inclusion. In particular, the increase of NEsOCur polarity (from 0.73 to 1.42) and the decrease of microviscosity (from 2.46 to 0.78), with respect to the empty ones (Rinaldi et al., 2022a), have been observed, probably due to the chemical structure of the loaded Curcumin. In fact, Curcumin molecules, dispersed in the oily droplet, could orient its hydroxyl groups near the head polar groups of the surfactant molecules with consequent rearrangement of the overall structure, promotion of water adsorption, perturbation of the oil droplet, increase of the polarity value and decrease of the microviscosity (Basu Ray et al., 2006; Feng and Liu, 2009; Sarheed et al., 2020; Vasilescu et al., 2011; Wakisaka et al., 2014).

pH sensitivity of NEsOCur was investigated also in terms of anisotropy, polarity and microviscosity variations. At pH 5.5 the excimer intensity increased (IE), revealing an increased microviscosity, as reported

Table 2
Physical-chemical features of nanoemulsions. The nanodroplets dimensions (Hydrodynamic Diameter), ζ-Potential, polydispersity index (PDI), and entrapped Curcumin % were evaluated at two different pH (7.4 and 7.5) to demonstrate the pH sensitiveness of NEsOCur at acidic pH.

Sample	Hydrodynamic Diameter (nm) ± SD		PDI ± SD		ζ-Potential (mV) ± SD		E.E % ± SD	
	pH 7.4	pH 5.5	pH 7.4	pH 5.5	pH 7.4	pH 5.5	pH 7.4	pH 5.5
NEsOCur	122 ± 4	382 ± 19	0.27 ± 0.01	0.38 ± 0.01	−42 ± 1	−28 ± 2	99 ± 1	98 ± 1

Data was obtained as the means of three independent experiments. Errors are the standard deviations (SD) of data.

Table 3
Nanoemulsions Anisotropy, Polarity and Microviscosity values (preparing the sample with pyrene and DPH as fluorescent probes). To demonstrate the pH sensitiveness of NEsOCur, the samples were analyzed at pH pH7,4 (employing Hepes buffer) and at pH 5,5 (employing acetate buffer). SD values are all in the range ± 0.01–0.02.

Sample		NEsOCur
Anisotropy	pH: 7.4	0.17
(Fluidity)	pH: 5.5	0.12
I1/I3	pH: 7.4	1.42
(Polarity)	pH: 5.5	1.30
IE/I3	pH: 7.4	0.78
(Microviscosity)	pH: 5.5	3.45

in Table 3. At this pH value, despite the increase of the hydrodynamic diameter, the surfactant tail rearrangement and the water adsorption in the nanocarrier reduce the available space for the pyrene probes (in monomer form), with consequent excimers formation (Winnik, 1993). All these investigated parameters (fluidity, polarity and microviscosity) are specific features that significantly could affect the *in vivo* behavior of the nanocarrier. In particular, the oil droplet rigidity, microviscosity and polarity play a critical role in the retention and release of the loaded drug by the nanocarriers, as well they could affect the NEs *in vivo* circulation time or its ability to interact with membranes or cells (Senior and Gregoriadis, 1982) . In detail, NEsOCur showed a low anisotropy and polarity values (at both pH), and these results indicate a quite fluid oil nanodroplet able to release the loaded drug (as demonstrated by release studies) and that could be able to efficiently interact with membranes or cells (Rinaldi et al., 2022a). Moreover, at pH 5,5 the rearrangement of the structure allows to an enhanced microviscosity of the oil nanodroplet that assure the maintained integrity of the NEsOCur, but the slight decrease of anisotropy value (inversely proportional with the rigidity) allows a higher release of the Curcumin with respect to pH 7,4 one (as described and discussed below in release studies section).

The morphological and dimensional changes of NEsOCur under different pH conditions, were visualized by TEM. As shown in Fig. 1, panel A, the NEsOCur incubated at pH 7.4 appears monodispersed and almost spherical in shape with size values in good agreement with DLS measurements. The surface of the nanodroplets shows a compact and homogeneous structure without signs of degradation. In contrast, NEsOCur incubated at pH 5.5 (Fig. 1, panel B) shows a deep modification, compared to their counterpart incubated at pH 7.4. The nanodroplets appear larger in size, in agreement with DLS results, due to a swelling process that also induces dramatic surface changes with non-homogeneous structure.

The nanodroplets seemed to maintain their spherical shape and not appear totally decomposed or collapsed (Fig. 1, panel B). The conserved shape and the appearance of holes agreed with results obtained in release experiments (Fig. 4). In fact, if the vesicles were destroyed or drastically damaged there would be an immediate release of the drug in large quantities and all at once. However, at pH 5.5 the vesicles still show a spherical shape, although larger in size, with the appearance of holes which allow the drug to escape slowly and not in all at once.

X-ray scattering experiments have been performed to characterize the structure of the samples on the nanometer length scale. NEsO and NEsOCur have been observed at pH 7.4 and the corresponding intensity profiles are reported in Fig. 2, panel A. Both systems showed a characteristic core-multishell pattern with an oily core surrounded by a thick shell, thicker than a single Tween 80 monolayer. The surfactant molecules, in high concentration, besides probably surrounding the core with a monolayer, formed at least one additional concentric bilayer. In the NEsO the characteristic internal distance between the coatings was about 10 nm. The loading of curcumin into NEsOCur changed the features of the intensity profile, indicating that curcumin was incorporated into the hydrophobic regions of the particle while preserving the overall core multi-shell arrangement of the structure. The analysis of the complex shell arrangement has been performed on NEsOCur at pH 7.4 and pH 5.5 by a multishell model. Results of the fit are reported in Fig. 2, panel B. The characteristic internal distance between the shells was about 15 nm at both pH values, definitely larger than the one observed in NEsO. The shells were modeled by the form factor of bilayers with a thickness of 6 nm at pH 7.4 and 4 nm at pH 5.5. This structural change suggests a partial destabilization of the amphiphilic coating of NEsOCur according to TEM and SAXS analyses.

The combination of multiple technique demonstrated that the Curcumin inclusion in the NEsO did not affect its overall integrity and pH-sensitivity respect to empty ones.

Stability studies were carried out for 90 days, storing NEsOCur at two different temperatures (25 °C, and 4 °C), to obtain information about the ideal storage temperature. The experiments were carried out evaluating the vesicle size and ζ-potential by DLS measurements as described in Section 2.8 and results were reported in Fig. 3. Stability studies on empty NEsO at two different temperatures were previously reported (Rinaldi et al., 2022a). No variations of hydrodynamic diameter or ζ-potential for NEsOCur have been detected when the sample is stored at room temperature (Fig. 3, panel A) while at 4 °C, an increase of hydrodynamic diameter characterized the sample starting from 30 days (Fig. 3, panel B). Probably, NEsOCur did not show good physical stability under long-term storage at 4 °C due to coalescence phenomena of nanodroplet, and thus size increasing. This result suggests that nanoemulsions were not suitable for temperature storage at 4 °C (Bi et al., 2023; Shi et al., 2022).

To evaluate Curcumin stability in terms of decomposition or degradation, the Curcumin (free and loaded) peak was detected by UV spectrophotometry. The UV spectra were recorded immediately after sample preparation and after 30, 60, and 90 days at room temperature and 4 °C.

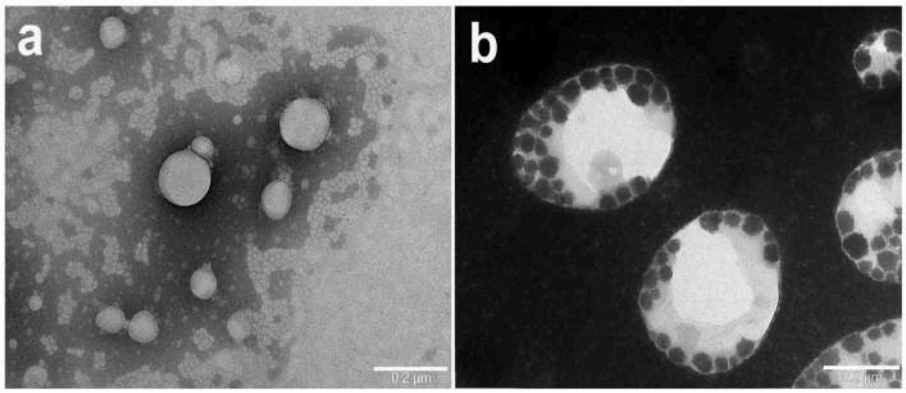

Fig. 1. Transmission electron micrographs of NEsOCur at pH 7.4 (A) and 5.5 (B). Vesicles were counterstained with PTA and observed as negative staining, by a FEI 280S transmission electron microscopy (FEI Company, Hillsboro, OR, USA), at an accelerating voltage of 100 kV.

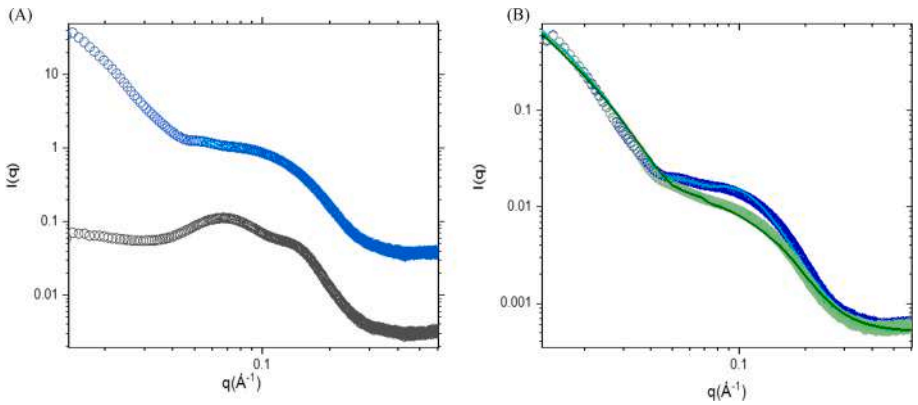

Fig. 2. A) SAXS intensity profiles of NEsO (black circles) and NEsOCur (blue circles) at pH 7.4 (the curves have been shifted vertically for sake of clarity). B) NEsOCur at pH 7.4 (blue circles) and 5.5 (green circles) with fit (solid lines). The buffer employed to prepare the samples have been Hepes buffer (pH 7,4) or acetate buffer (pH 5,5).

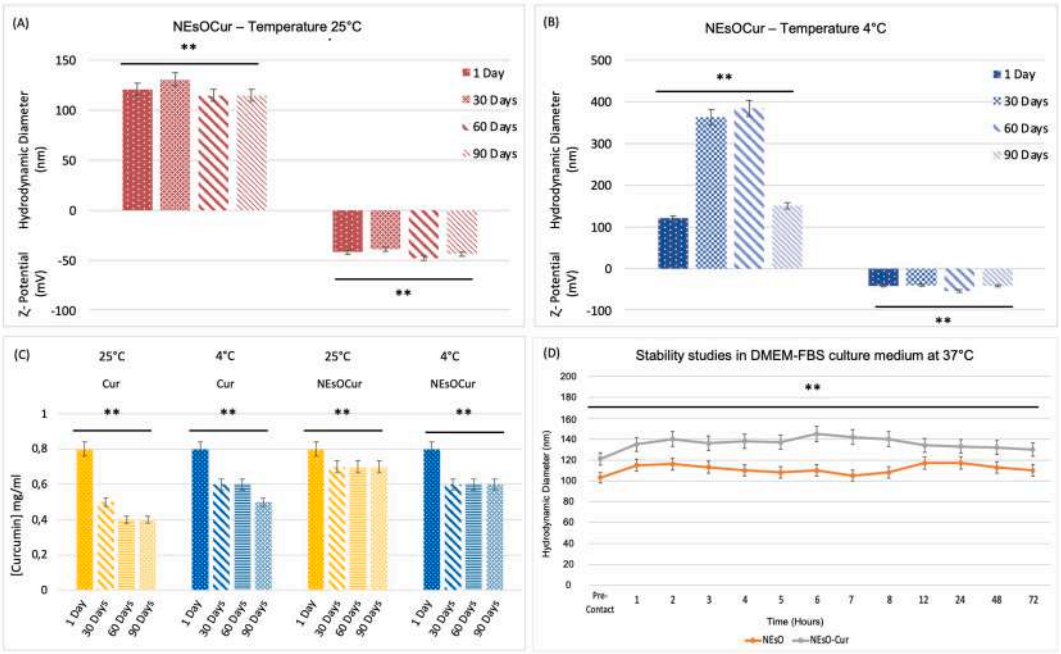

Fig. 3. Physical-chemical stability of NEsO and NEsOCur: stability studies of NEsOCur in terms of hydrodynamic diameter and ζ-potential variations until up 90 days at room temperature (panel A) and 4 °C (panel B). Stability studies over time of free Curcumin (Cur) and Curcumin in NEsO (NEsOCur) at two different storage temperatures over a 90-day period (panel C) were obtained by UV–vis spectrophotometer. Stability studies of NEsOCur in terms of hydrodynamic diameter and ζ-potential in DMEM-FBS (D). To obtain size and ζ-potential values (panel A-B-D) the samples were analyzed by using DLS. The hydrodynamic diameter was obtained by intensity distributions measures, and the ζ-potential value obtained by distribution curves. Data were obtained as the mean of three independent experiments. * $p < 0.05$, ** $p < 0.01$, *** $p < 0.001$.

As shown in Fig. 3, panel C, it was possible to conclude that the inclusion of Curcumin in NEsO increases its stability. In fact, the concentration of the natural compound remained constant over time when it was loaded into NEsO and stored at room temperature.

The stability of NEsO and NEsOCur was also evaluated at 37 °C in a DMEM-FBS culture medium (Fig. 3, panel D). No significant alterations in average size were observed, evaluating hydrodynamic diameter and performing measurements at different time points (every hour for 8 h and then after 12, 24, 48 and 72 h) so it is possible to conclude that NEsO and NEsOCur are stable and resistant in this culture medium.

In vitro release studies of Curcumin from NEsOCur were conducted at two different pH (pH 7.4 and 5.5) for 8 h (until up 72 h see Figure S2) as described in section 2.11. In Fig. 4, it is possible to observe that Cur release is strongly influenced by the external pH. In particular, in acetate buffer (pH 5.5) the amount of released Curcumin is higher than that at pH 7.4 (approximately 60 % vs 40 %). These results confirm the pH sensitivity of the nanoemulsions due to NEsOCur destabilization at pH 5.5.

The NEsOCur were tested on the B16F10, a murine melanoma cell line originating from C57BL/6J mice. To determine if NEsOCur could deliver Curcumin, cellular internalization studies were carried out, exploiting Cur autofluorescence emission at 525 nm wavelength (FITC). Therefore, the B16F10 cells were treated with two amounts of nano-emulsions corresponding to Curcumin concentrations of 6.75 and 13.5 μM, in agreement with literature data (Mirzaei et al., 2016) for different culture times (5 h, 24 h, and 48 h) and in parallel, as a positive control, with the same doses of Curcumin dissolved in DMSO (referred as free Cur). By flow cytometry analysis, it is possible to observe that 5 h of exposure to NEsOCur (Fig. 5A) followed by 24 h of culture were sufficient to detect Curcumin fluorescence as compared to the CTR, but not

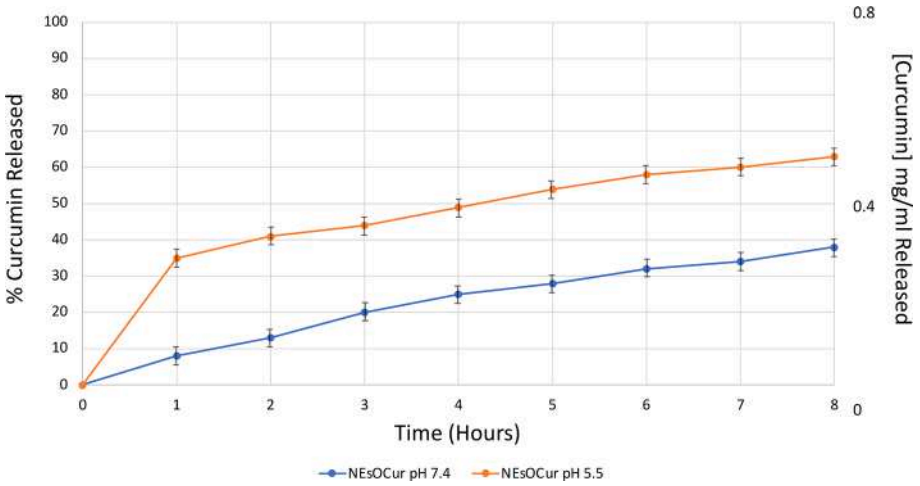

Fig. 4. Curcumin release profile until up to 8 h preparing the samples in Hepes buffer (pH 7.4, 0.02 M) and Acetate buffer (pH 5.5, 0.2 M), to demonstrate the pH sensitiveness of the samples, were performed by spectrophotometer. Blue line and orange line represent the curcumin released respectively by sample NEsOCur at pH 7,4 and 5,5. Data were obtained as the mean of three independent experiments.

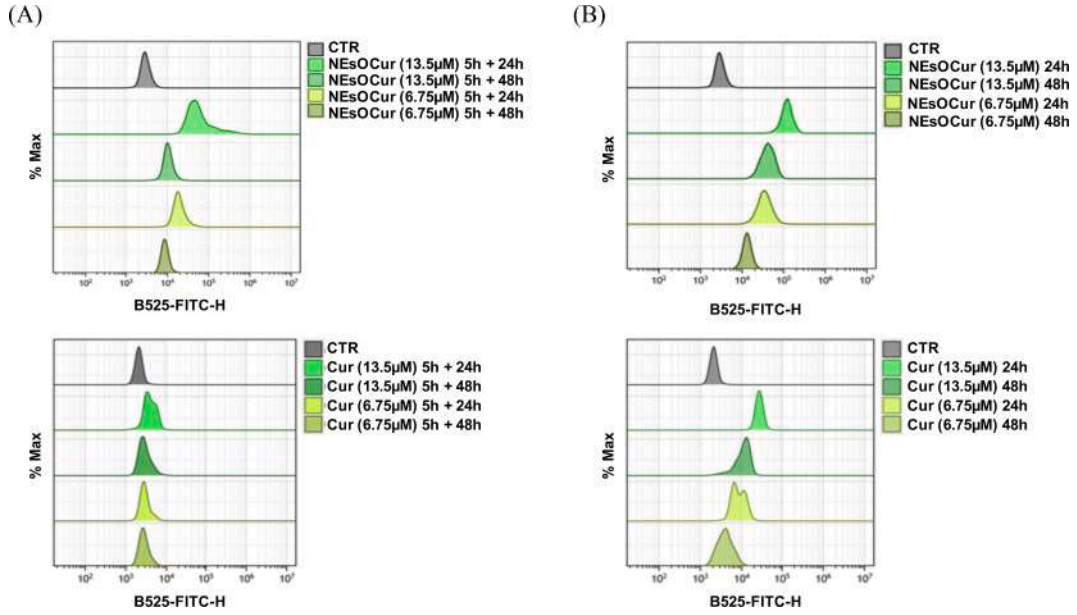

Fig. 5. Evaluation of Curcumin internalization in B16F10 cells, conveyed by NEsO (top panel) or dissolved in DMSO (free Cur, bottom) by FCM analysis of fluorescence emission at wavelength for FITC (525 nm). The legend reported on the right of plot shows the concentration of Curcumin used and the treatment time. It has been evaluated the long-lasting maintenance of Cur inside the cells (A) after a short treatment (5 h) followed by 24 and 48 h of culture or (B) continuously during 24 and 48 h of culture. A representative experiment out of three is shown.

enough after 48 h when the fluorescent emission was almost undetectable. However, if the cells were continuously exposed to NEsOCur or free Cur, the fluorescence signal was well detectable at 24 h and still observable at 48 h, although reduced to less than half (Fig. 5B). Similar results have been obtained in B16F10 by using NEsO loaded with Nile Red, a red fluorescent stain for intracellular lipids (data not shown). As expected, the intensity of the fluorescent signal and the retention of Curcumin inside the cells were directly proportional to the amount of nanocarrier employed. The decrease in fluorescence over time is compatible with the cellular metabolism of Curcumin and the physiological fluorescence dilution among dividing cells. Interestingly, in all the treatments, Curcumin's internalization and retention were more effective when delivered by NEsO. Furthermore, the signal of internalized NEsOCur, suggests a more slow and gradual release of Curcumin entrapped in NEsO as compared with free Curcumin (Fig. 6).

In vitro and *in vivo* studies have shown that Curcumin acts as an anticancer agent, blocking the cell cycle and favoring apoptosis of the tumor cells (Mirzaei et al., 2016). As regards the B16F10 cell line, different studies showed that a concentration of at least 10 μM of Curcumin was required to inhibit their proliferation (Wolnicka-Glubisz et al., 2015). Therefore, was evaluated the cell growth influence of Curcumin loaded in the NEsO and to do that, B16F10 cells were cultured for different time points and in the presence of increasing doses of Curcumin, conveyed by NEsO or dissolved in DMSO, and the cell growth assessed by XTT assay. As shown in Fig. 7A and B, the results demonstrated that NEsOCur as well as free Cur, reduced the cell proliferative rate in a time and concentration-dependent manner (Fig. 8A), compared with control (CTR). As expected, starting from 48 h of treatment, 13.5 μM of Cur was highly effective in both conditions. As regards the lower doses, Cur entrapped by NEsO showed a stronger inhibitory effect, as showed by 4.5 μM of Cur, able to halve cell growth compared to CTR after 72 h of treatment. These results are consistent with the literature

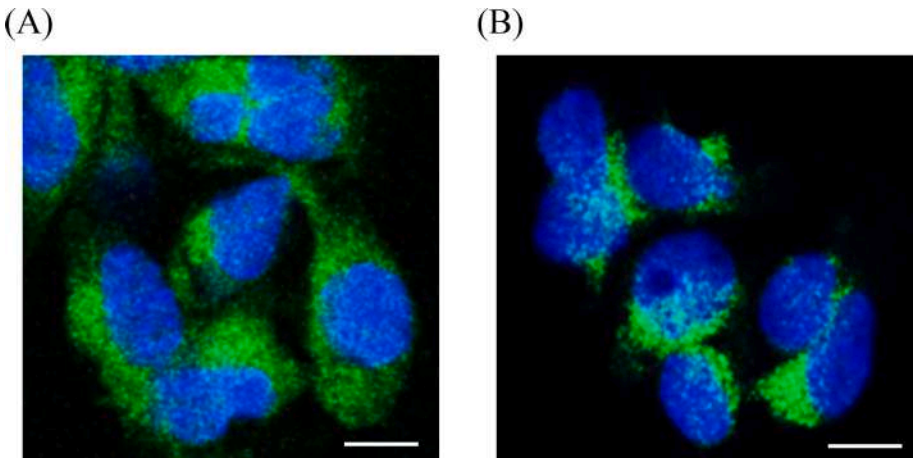

Fig. 6. Confocal microscopy analysis of intracellular distribution of Curcumin conveyed by NEsO (A) or dissolved in DMSO (B). B16F10 cells were treated for 24 h of culture with 13.5 μM of Cur. Nuclei were stained with Hoechst 33.342 (blue). Curcumin fluorescence signal showed the same pattern of distribution regardless of the mode of administration. Microscopic pictures represent a merge between green (Curcumin) and blue fluorescence images. Bar, 10 μm. A representative experiment out of three is shown.

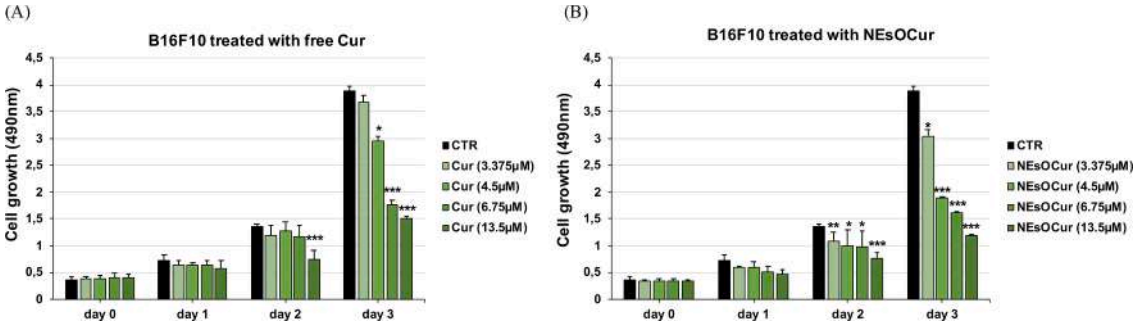

Fig. 7. Evaluation of Curcumin effect on B16F10 cells growth. The B16F10 melanoma cell line was treated with different concentrations of Cur, as indicated in the respective legend, for up to 3 days continuously. Intracellular Curcumin conveyed by NEsO influences B16F10 growth at different concentrations (B). The inhibitory effect on proliferation was comparable to that observed with Curcumin in DMSO (A). Cell growth was measured at each time point (day 0—3) using an XTT assay. Data are represented as mean ± SD of at least three independent experiments. * $p < 0.05$, ** $p < 0.01$, *** $p < 0.001$ compared with the control cells.

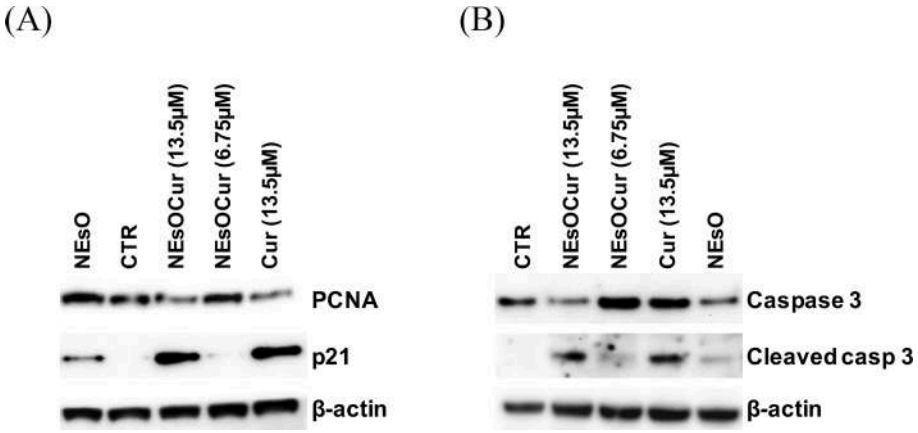

Fig. 8. Western blot analysis of total proteins extracted from B16F10 cells treated for 48 h with NEsOCur (6.75 and 13.5 μM), Cur free (13.5 μM) and NEsO (amount equivalent to 13.5 μM Cur one). The expression of p21, a negative modulator of the cell cycle progression, of PCNA, a proliferative marker, and cleaved caspase 3, a positive modulator of the apoptotic program was investigated. As shown in (A), cells treated with 13.5 μM of Cur displayed p21 upregulation paralleled by PCNA down-modulation respect to control (CTR), in agreement with cell growth reduction. In the same samples, analysis of caspase and cleaved caspase (B), revealed a strong activation of caspase 3 in the cells treated with 13.5 μM of Cur respect to the relative empty NEsO and CTR, in line with the pro-apoptotic activity of Curcumin. β-actin was used as a loading control. A representative experiment out of three is shown.

and suggest that Curcumin delivered by NEsO has a higher efficacy, possibly ensured by both the protection from degradation outside the cell and an efficient intracellular uptake and release.

Concerning human melanoma, Zhang YP and coworkers determined the proliferation rate of A375 cells in the presence of increasing concentrations of Curcumin after 48 h of treatment and calculated the half-

maximal inhibitory concentration (IC50) at 10.05 μM (Zhang et al., 2015). After verifying their ability in Cur internalization delivered by NEsOCur (Figure S1A), cell proliferation assays were carried out in the A375M cells, a metastatic clone derived by A375 cells, previously used to test the different formulations of OA-nanoemulsions (Rinaldi et al., 2022a). Interestingly, it was observed that, unlike B16F10, the growth of these cells was unaffected by the two lower concentrations of Curcumin utilized at each time point analyzed (Figure S1B). Conversely, 13.5 μM of Cur was already effective after 24 h of treatment and maintained a strong inhibitory activity against cell proliferation in the following 48 and 72 h. Interestingly, at 72 h we observed a decrease of about 50 % of cell proliferation both with 13.5 μM and 6.75 μM of Cur. These results suggest the necessity of a longer time to obtain a sharp cell growth block. In this regard, it is important to highlight that A375M cells have a higher malignant character compared to A375 and B16F10, which may give them greater resistance to the inhibitory stimuli induced by lower concentrations of Curcumin.

To deeply study at a molecular level the cell growth inhibition, the expression of some factors involved in the cell cycle was investigated. Therefore, the attention was focused on the cyclin-dependent kinase inhibitor p21 (also known as p21WAF1/Cip1) as a negative modulator of the cell cycle, and the Proliferating Cell Nuclear Antigen (PCNA), a marker for cell proliferation, both misregulated in several cancers and modulated by Curcumin (Dahmke et al., 2013; Gogada et al., 2011). Additionally, several studies demonstrated that Curcumin beyond stopping cell cycle progression, can trigger apoptosis (Srivastava et al., 2007). Caspases, in particular the cleaved caspase 3, play a crucial role in dismantling the dying cell (Hussar, 2022) at the onset of the apoptotic program. Therefore, western blot analysis on B16F10 cells treated with NEsOCur and free Cur after 48 h of treatment were performed and Curcumin treatment at 13.5 μM, either conveyed by NEsO or free caused an upregulation of p21 and downregulation of PCNA (Fig. 8A), compared to untreated and treated cells with an equivalent amount of NEsO, providing evidence of the cell cycle arrest in response to Curcumin stimulus conveyed by NEsO. Finally, analysis of caspase 3 expression showed its activation in these samples, in line with the pro-apoptotic role of curcumin. Therefore, the upregulation of p21 accompanied by downmodulation of PCNA, and activation of Caspase 3, greatly support the NEsO as an effective carrier of biologically active Curcumin.

Overall, it was highlighted that NEsOCur is highly effective in loading Curcumin and in releasing it into the cell while maintaining its physical and chemical properties over time. Furthermore, this new formulation could improve the bioavailability of Curcumin by overcoming its low solubility and degradation. Curcumin demonstrated rapid internalization and intracellular retention resulting in biological effects on cell proliferation and induction of apoptosis, as demonstrated in various cellular models. This study marks the first step towards developing NEsO prepared with new lipophilic drugs, making it possible to use them at reduced concentrations without compromising their efficacy, for future *in vivo* studies. In this view, according to our published data on human fibroblasts derived from skin biopsies (Rinaldi et al., 2022), no evidence of growth inhibition was found in human keratinocyte cell line (HaCaT) when treated with two different amounts of NEsO (Figure S3). More importantly, the same doses of NEsO were injected in mice intravenously twice a week for about 20 days without observing any toxicity (data not shown), supporting their usefulness as drug nanocarriers for *in vivo* experimental models.

4. Conclusion

In this work, a pH-sensitive Oleic Acid-based Nanoemulsion has been developed and deeply characterized thanks to a multidisciplinary approach. The obtained results indicate NEsO as a good candidate to load Curcumin, chosen in this work as a good model of lipophilic drug with antitumoral properties. Curcumin is efficiently entrapped (almost 100 %) and protected from degradation. The obtained nanosystem is quite stable, especially at room temperature and shows pH-sensitivity, as demonstrated by different experiments. Indeed, Curcumin, delivered by NEsO, can affect cell proliferation and induce comparable and sometimes higher apoptosis onset in comparison to free Curcumin. These studies, therefore, open the way towards the development of NEsO prepared with lipophilic drugs potentially effective against melanoma. These formulations will present a double advantage, as they will offer a route of administration of oleic acid, endowed with an anti-metastatic role, together with the loaded drug, and will bypass the absence of a specific molecular target for melanoma. In conclusion, all these results highlight the potentiality of NEsO to deliver and selectively release lipophilic drugs in the acidified tumoral microenvironment in *in vivo* studies.

Ethical statement

The study was conducted in compliance with the current ethical guidelines of the Italian authority and according to the Declaration of Helsinki Principles.

Funding

This research was funded by “Progetti per Avvio alla Ricerca – Tipo 1” – Numero protocollo: AR1221816739E49F. “pH-responsive Oleic Acid based nanoemulsions: preparation, characterization and *in vitro* applications.” – Jacopo Forte, and by Grant BB29 from Ricerca Indipendente ISS 2020-22 –Gianfranco Mattia, project code: ISS20-027716d9053a “A novel combination of nanotechnologies to potentiate antitumor cytotoxic activity in a murine model of melanoma: a view on sex implication in immune response”.

CRediT authorship contribution statement

Jacopo Forte: Writing – review & editing, Writing – original draft, Funding acquisition, Data curation, Conceptualization. **Maria Gioia Fabiano:** Investigation, Formal analysis. **Maria Grazia Ammendolia:** Investigation, Formal analysis, Data curation. **Rossella Puglisi:** Writing – review & editing, Writing – original draft, Validation, Data curation, Conceptualization. **Federica Rinaldi:** Writing – review & editing, Writing – original draft, Validation, Supervision, Investigation, Data curation, Conceptualization. **Caterina Ricci:** Writing – original draft, Investigation, Formal analysis, Data curation. **Elena Del Favero:** Writing – original draft, Investigation, Formal analysis, Data curation. **Maria Carafa:** Writing – review & editing, Writing – original draft, Validation, Supervision, Conceptualization. **Gianfranco Mattia:** Writing – review & editing, Writing – original draft, Validation, Supervision, Funding acquisition, Data curation, Conceptualization. **Carlotta Marianecci:** Writing – review & editing, Writing – original draft, Validation, Supervision, Conceptualization.

Declaration of competing interest

The authors declare that they have no known competing financial interests or personal relationships that could have appeared to influence the work reported in this paper.

Data availability

Data will be made available on request.

Appendix A. Supplementary material

Supplementary data to this article can be found online at https://doi.org/10.1016/j.ijpharm.2024.124380.

References

Barattin, M., Mattarei, A., Balasso, A., Paradisi, C., Cantù, L., Del Favero, E., Viitala, T., Mastrotto, F., Caliceti, P., Salmaso, S., 2018. pH-controlled liposomes for enhanced cell penetration in tumor environment. ACS Appl. Mater. Interfaces 10, 17646–17661. https://doi.org/10.1021/acsami.8b03469.

Basu Ray, G., Chakraborty, I., Moulik, S.P., 2006. Pyrene absorption can be a convenient method for probing critical micellar concentration (cmc) and indexing micellar polarity. J. Colloid Interface Sci. 294, 248–254. https://doi.org/10.1016/j.jcis.2005.07.006.

Bellenghi, M., Puglisi, R., Pedini, F., De Feo, A., Felicetti, F., Bottero, L., Sangaletti, S., Errico, M.C., Petrini, M., Gesumundo, C., Denaro, M., Felli, N., Pasquini, L., Tripodo, C., Colombo, M.P., Carè, A., Mattia, G., 2015 Jul. SCD5-induced oleic acid production reduces melanoma malignancy by intracellular retention of SPARC and cathepsin B. J Pathol. 236 (3), 315–325. https://doi.org/10.1002/path.4535. Epub 2015 Apr 20 PMID: 25802234.

Bi, D., Li, M., Yao, L., Zhu, N., Fang, W., Guo, W., Wu, Y., Xu, H., Hu, Z., Xu, X., 2023. Enhancement of the chemical stability of nanoemulsions loaded with curcumin by unsaturated mannuronate oligosaccharide. Food Chem. 414, 135670 https://doi.org/10.1016/j.foodchem.2023.135670.

Dahmke, I.N., Backes, C., Rudzitis-Auth, J., Laschke, M.W., Leidinger, P., Menger, M.D., Meese, E., Mahlknecht, U., 2013. Curcumin intake affects miRNA signature in murine melanoma with mmu-miR-205-5p Most significantly altered. PLoS One 8, e81122.

Dwivedi, M., Buske, J., Haemmerling, F., Blech, M., Garidel, P., 2020. Acidic and alkaline hydrolysis of polysorbates under aqueous conditions: towards understanding polysorbate degradation in biopharmaceutical formulations. Eur. J. Pharm. Sci. 144, 105211 https://doi.org/10.1016/j.ejps.2019.105211.

Feng, J.-Y., Liu, Z.-Q., 2009. Phenolic and enolic hydroxyl groups in curcumin: which plays the major role in scavenging radicals? J. Agric. Food Chem. 57, 11041–11046. https://doi.org/10.1021/jf902244g.

Forte, J., Hanieh, P.N., Poerio, N., Olimpieri, T., Ammendolia, M.G., Fraziano, M., Fabiano, M.G., Marianecci, C., Carafa, M., Bordi, F., Sennato, S., Rinaldi, F., 2023. Mucoadhesive Rifampicin-liposomes for the treatment of pulmonary infection by mycobacterium abscessus: chitosan or ε-poly-L-lysine decoration. Biomolecules 13, 924. https://doi.org/10.3390/biom13060924.

Gogada, R., Amadori, M., Zhang, H., Jones, A., Verone, A., Pitarresi, J., Jandhyam, S., Prabhu, V., Black, J.D., Chandra, D., 2011. Curcumin induces Apaf-1-dependent, p21-mediated caspase activation and apoptosis. Cell Cycle 10, 4128–4137. https://doi.org/10.4161/cc.10.23.18292.

Hussar, P., 2022. Apoptosis regulators Bcl-2 and caspase-3. Encyclopedia 2, 1624–1636. https://doi.org/10.3390/encyclopedia2040111.

Jessurun, C.A.C., Vos, J.A.M., Limpens, J., Luiten, R.M., 2017. Biomarkers for response of melanoma patients to immune checkpoint inhibitors: a systematic review. Front. Oncol. 7.

Ke, D., Wang, X., Yang, Q., Niu, Y., Chai, S., Chen, Z., An, X., Shen, W., 2011. Spectrometric study on the interaction of dodecyltrimethylammonium bromide with curcumin. Langmuir 27, 14112–14117. https://doi.org/10.1021/la203592j.

Kunwar, A., Barik, A., Mishra, B., Rathinasamy, K., Pandey, R., Priyadarsini, K.I., 2008. Quantitative cellular uptake, localization and cytotoxicity of curcumin in normal and tumor cells. Biochimica et Biophysica Acta (BBA) - General Subjects 1780, 673–679. doi: 10.1016/j.bbagen.2007.11.016.

Le Guyader, L., Le Roux, C., Mazères, S., Gaspard-Iloughmane, H., Gornitzka, H., Millot, C., Mingotaud, C., Lopez, A., 2007. Changes of the membrane lipid organization characterized by means of a new cholesterol-pyrene probe. Biophys. J . 93, 4462–4473. https://doi.org/10.1529/biophysj.107.112821.

Lentz, B.R., 1989. Membrane "fluidity" as detected by diphenylhexatriene probes. Chem. Phys. Lipids 50, 171–190. https://doi.org/10.1016/0009-3084(89)90049-2.

Liu, Q., Loo, W.T.Y., Sze, S.C.W., Tong, Y., 2009. Curcumin inhibits cell proliferation of MDA-MB-231 and BT-483 breast cancer cells mediated by down-regulation of NFκB, cyclinD and MMP-1 transcription. Phytomedicine 16, 916–922. https://doi.org/10.1016/j.phymed.2009.04.008.

Lu, Y., Wei, C., Xi, Z., 2014. Curcumin suppresses proliferation and invasion in non-small cell lung cancer by modulation of MTA1-mediated Wnt/β-catenin pathway. In Vitro Cell. Dev. Biol. -Animal 50, 840–850. https://doi.org/10.1007/s11626-014-9779-5.

Makhathini, S.S., Omolo, C.A., Kiruri, L.W., Walvekar, P., Devnarain, N., Mocktar, C., Govender, T., 2022. Synthesis of pH-responsive dimethylglycine surface-modified branched lipids for targeted delivery of antibiotics. Chem. Phys. Lipids 249, 105241. https://doi.org/10.1016/j.chemphyslip.2022.105241.

Manosroi, A., Wongtrakul, P., Manosroi, J., Sakai, H., Sugawara, F., Yuasa, M., Abe, M., 2003. Characterization of vesicles prepared with various non-ionic surfactants mixed with cholesterol. Colloids Surf. BBiointerfaces 30, 129–138. https://doi.org/10.1016/S0927-7765(03)00080-8.

Mirzaei, H., Naseri, G., Rezaee, R., Mohammadi, M., Banikazemi, Z., Mirzaei, H.R., Salehi, H., Peyvandi, M., Pawelek, J.M., Sahebkar, A., 2016. Curcumin: A new candidate for melanoma therapy? Int. J. Cancer 139, 1683–1695. https://doi.org/10.1002/ijc.30224.

Pandey, M., Choudhury, H., Gorain, B., Tiong, S.Q., Wong, G.Y.S., Chan, K.X., They, X., Chieu, W.S., 2021. Site-specific vesicular drug delivery system for skin cancer: a novel approach for targeting. Gels 7, 218. https://doi.org/10.3390/gels7040218.

Parchekani, J., Allahverdi, A., Taghdir, M., Naderi-Manesh, H., 2022. Design and simulation of the liposomal model by using a coarse-grained molecular dynamics approach towards drug delivery goals. Sci Rep 12, 2371. https://doi.org/10.1038/s41598-022-06380-8.

Prajapati, I., Peters, B.-H., Larson, N.R., Wei, Y., Choudhary, S., Kalonia, C., Hudak, S., Esfandiary, R., Middaugh, C.R., Schöneich, C., 2020. Cis/trans isomerization of unsaturated fatty acids in polysorbate 80 during light exposure of a monoclonal antibody-containing formulation. J. Pharm. Sci. 109, 603–613. https://doi.org/10.1016/j.xphs.2019.10.068.

Puglisi, R., Bellenghi, M., Pontecorvi, G., Gulino, A., Petrini, M., Felicetti, F., Bottero, L., Mattia, G., Carè, A., 2018. SCD5 restored expression favors differentiation and epithelial-mesenchymal reversion in advanced melanoma. Oncotarget 9, 7567–7581. https://doi.org/10.18632/oncotarget.24085.

Qiu, Y., Yu, T., Wang, W., Pan, K., Shi, D., Sun, H., 2014. Curcumin-induced melanoma cell death is associated with mitochondrial permeability transition pore (mPTP) opening. Biochem. Biophys. Res. Commun. 448, 15–21. https://doi.org/10.1016/j.bbrc.2014.04.024.

Rambow, F., Marine, J.-C., Goding, C.R., 2019. Melanoma plasticity and phenotypic diversity: therapeutic barriers and opportunities. Genes Dev. 33, 1295–1318. https://doi.org/10.1101/gad.329771.119.

Rinaldi, F., Forte, J., Pontecorvi, G., Hanieh, P.N., Carè, A., Bellenghi, M., Tirelli, V., Ammendolia, M.G., Mattia, G., Marianecci, C., Puglisi, R., Carafa, M., 2022a. pH-responsive oleic acid based nanocarriers: melanoma treatment strategies. Int. J. Pharm. 613, 121391 https://doi.org/10.1016/j.ijpharm.2021.121391.

Rinaldi, F., Hanieh, P.N., Maurizi, L., Longhi, C., Uccelletti, D., Schifano, E., Del Favero, E., Cantù, L., Ricci, C., Ammendolia, M.G., Paolino, D., Froiio, F., Marianecci, C., Carafa, M., 2022b. Neem oil or almond oil nanoemulsions for vitamin E delivery: from structural evaluation to in vivo assessment of antioxidant and anti-inflammatory activity. Int J Nanomedicine 17, 6447–6465. https://doi.org/10.2147/IJN.S376750.

Rosner, K., Röpke, C., Pless, V., Skovgaard, G.L., 2006. Late type apoptosis and apoptosis free lethal effect of quercetin in human melanoma. Biosci. Biotech. Bioch. 70, 2169–2177. https://doi.org/10.1271/bbb.60129.

Sarheed, O., Dibi, M., Ramesh, K.V.R.N.S., 2020. Studies on the effect of oil and surfactant on the formation of alginate-based O/W lidocaine nanocarriers using nanoemulsion template. Pharmaceutics 12, 1223. https://doi.org/10.3390/pharmaceutics12121223.

Sciolla, F., Truzzolillo, D., Chauveau, E., Trabalzini, S., Di Marzio, L., Carafa, M., Marianecci, C., Sarra, A., Bordi, F., Sennato, S., 2021. Influence of drug/lipid interaction on the entrapment efficiency of isoniazid in liposomes for antitubercular therapy: a multi-faced investigation. Colloids Surf. BBiointerfaces 208, 112054. https://doi.org/10.1016/j.colsurfb.2021.112054.

Senior, J., Gregoriadis, G., 1982. Is half-life of circulating liposomes determined by changes in their permeability? FEBS Lett. 145, 109–114. https://doi.org/10.1016/0014-5793(82)81216-7.

Sennato, S., Bordi, F., Cametti, C., Coluzza, C., Desideri, A., Rufini, S., 2005. Evidence of domain formation in cardiolipin−glycerophospholipid mixed monolayers. A thermodynamic and AFM study. J. Phys. Chem. B 109, 15950–15957. https://doi.org/10.1021/jp051893q.

Shi, Y., Zhang, M., Chen, K., Wang, M., 2022. Nano-emulsion prepared by high pressure homogenization method as a good carrier for Sichuan pepper essential oil: Preparation, stability, and bioactivity. LWT 154, 112779. https://doi.org/10.1016/j.lwt.2021.112779.

Song, M., Liu, C., Chen, S., Zhang, W., 2021. Nanocarrier-based drug delivery for melanoma therapeutics. Int. J. Mol. Sci. 22, 1873. https://doi.org/10.3390/ijms22041873.

Srivastava, R.K., Chen, Q., Siddiqui, I., Sarva, K., Shankar, S., 2007. Linkage of curcumin-induced cell cycle arrest and apoptosis by cyclin-dependent kinase inhibitor p21/WAF1/CIP1. Cell Cycle 6, 2953–2961. https://doi.org/10.4161/cc.6.23.4951.

Stefanidis, D., Jencks, W.P., 1993. General base catalysis of ester hydrolysis. J. Am. Chem. Soc. 115, 6045–6050. https://doi.org/10.1021/ja00067a020.

Stubbs, M., McSheehy, P.M.J., Griffiths, J.R., Bashford, C.L., 2000. Causes and consequences of tumour acidity and implications for treatment. Mol. Med. Today 6, 15–19. https://doi.org/10.1016/S1357-4310(99)01615-9.

Tomeh, M., Hadianamrei, R., Zhao, X., 2019. A review of curcumin and its derivatives as anticancer agents. IJMS 20, 1033. https://doi.org/10.3390/ijms20051033.

Vasilescu, C., Drob, P., Vasilescu, E., Demetrescu, I., Ionita, D., Prodana, M., Drob, S.I., 2011. Characterisation and corrosion resistance of the electrodeposited hydroxyapatite and bovine serum albumin/hydroxyapatite films on Ti–6Al–4V–1Zr alloy surface. Corros. Sci. 53, 992–999. https://doi.org/10.1016/j.corsci.2010.11.033.

Wakisaka, Y., Ago, T., Kamouchi, M., Kuroda, J., Matsuo, R., Hata, J., Gotoh, S., Isomura, T., Awano, H., Suzuki, K., Fukuda, K., Okada, Y., Kiyohara, Y., Ooboshi, H., Kitazono, T., 2014. Plasma S100A12 is associated with functional outcome after ischemic stroke: research for Biomarkers in Ischemic stroke. J. Neurol. Sci. 340, 75–79. https://doi.org/10.1016/j.jns.2014.02.031.

Wang, K., Fan, H., Chen, Q., Ma, G., Zhu, M., Zhang, X., Zhang, Y., Yu, J., 2015. Curcumin inhibits aerobic glycolysis and induces mitochondrial-mediated apoptosis through hexokinase II in human colorectal cancer cells in vitro. Anticancer Drugs 26, 15. https://doi.org/10.1097/CAD.0000000000000132.

Whiteside, T.L., 2008. The tumor microenvironment and its role in promoting tumor growth. Oncogene 27, 5904–5912. https://doi.org/10.1038/onc.2008.271.

Winnik, F.M., 1993. Photophysics of preassociated pyrenes in aqueous polymer solutions and in other organized media. Chem. Rev. 93, 587–614. https://doi.org/10.1021/cr00018a001.

Wolnicka-Glubisz, A., Nogal, K., Żądło, A., Płonka, P.M., 2015. Curcumin does not switch melanin synthesis towards pheomelanin in B16F10 cells. Arch Dermatol Res 307, 89–98. https://doi.org/10.1007/s00403-014-1523-1.

Xue, X., Yu, J.-L., Sun, D.-Q., Kong, F., Qu, X.-J., Zou, W., Wu, J., Wang, R.-M., 2014. Curcumin induces apoptosis in SGC-7901 gastric adenocarcinoma cells via

regulation of mitochondrial signaling pathways. Asian Pac. J. Cancer Prev. 15, 3987–3992. https://doi.org/10.7314/APJCP.2014.15.9.3987.
Zachariasse, K.A., 1978. Intramolecular excimer formation with diarylalkanes as a microfluidity probe for sodium dodecyl sulphate micelles. Chem. Phys. Lett. 57, 429–432. https://doi.org/10.1016/0009-2614(78)85541-9.
Zhang, Y.P., Li, Y.Q., Lv, Y.T., Wang, J.M., 2015. Effect of curcumin on the proliferation, apoptosis, migration, and invasion of human melanoma A375 cells. Genet. Mol. Res. 14, 1056–1067. https://doi.org/10.4238/2015.February.6.9.